Constraints on the Late Holocene Anthropogenic Contribution to the Atmospheric Methane Budget

Logan Mitchell *et al.*

Science **342**, 964 (2013);
DOI: 10.1126/science.1238920

Science (print ISSN 0036-8075; online ISSN 1095-9203) is published weekly, except the last week in December, by the American Association for the Advancement of Science, 1200 New York Avenue NW, Washington, DC 20005.

Constraints on the Late Holocene Anthropogenic Contribution to the Atmospheric Methane Budget

Logan Mitchell,[1]* Ed Brook,[1] James E. Lee,[1] Christo Buizert,[1] Todd Sowers[2]

The origin of the late preindustrial Holocene (LPIH) increase in atmospheric methane concentrations has been much debated. Hypotheses invoking changes in solely anthropogenic sources or solely natural sources have been proposed to explain the increase in concentrations. Here two high-resolution, high-precision ice core methane concentration records from Greenland and Antarctica are presented and are used to construct a high-resolution record of the methane inter-polar difference (IPD). The IPD record constrains the latitudinal distribution of emissions and shows that LPIH emissions increased primarily in the tropics, with secondary increases in the subtropical Northern Hemisphere. Anthropogenic and natural sources have different latitudinal characteristics, which are exploited to demonstrate that both anthropogenic and natural sources are needed to explain LPIH changes in methane concentration.

The 2.5-fold increase in the concentration of atmospheric methane (CH_4) since the start of the Industrial Revolution has accounted for ~20% of the total increase in radiative forcing over that time and motivated efforts to understand both natural CH_4 biogeochemistry and anthropogenic impacts on CH_4 sources and sinks (*1*). There has been a lively debate about the impact of early human activities on the global CH_4 budget, stimulated by the observation that atmospheric CH_4 levels generally follow 30°N summer solar insolation over the past 800,000 years, but in the mid-Holocene [~5000 years ago (ka)] there is a divergence, with CH_4 increasing and insolation decreasing. The "early anthropogenic hypothesis" postulates that human activities were responsible for the increase in CH_4 since the mid-Holocene (and CO_2 increases since ~7 ka) (*2*), but others argue that the increase originates from natural sources (*3*). Archaeological evidence supports the hypothesis about early anthropogenic emissions, particularly from rice agriculture (*4*, *5*), although the magnitude of those emissions is debated (*3*, *6*).

One tool for understanding CH_4 budget changes is the CH_4 Inter-Polar Difference (IPD) (*7*–*9*), which can be reconstructed from polar ice cores. The IPD is a function of the latitudinal distribution of sources and sinks, as well as the interhemispheric mixing time. The prevalence of Northern Hemisphere (NH) sources leads to a positive IPD, with higher CH_4 levels recorded in Greenland ice cores than in Antarctic ones. Recent work has shown that the main CH_4 sink (OH) is stable on a range of time scales (*10*–*12*), and we have assumed that there have been no changes in the spatial distribution of OH in the late preindustrial Holocene (LPIH). Because interhemispheric transport has a second-order effect on the IPD (*13*), source changes are left as the dominant control on IPD variation. Because ~95% of humans lived in the NH tropics and subtropics (0° to 60°N) during the LPIH (*14*), the fingerprint of anthropogenic emissions would have been an increased IPD relative to the natural background. Indeed, NH anthropogenic emissions in the industrial age have increased the IPD to ~125 parts per billion (ppb) (~7.5% of the mean global concentration), far above the 42 ppb preindustrial background (~6.4% of the mean global concentration). Here we present decadally resolved ice core CH_4 records from the West Antarctic Ice Sheet (WAIS) Divide and the Greenland Ice Sheet Project 2 (GISP2) ice cores, which we use to reconstruct the IPD from 800 B.C.E. to 1800 C.E. (Fig. 1), thus providing data-driven constraints on the early anthropogenic hypothesis.

Our high-precision CH_4 measurements [pooled standard deviation (SD ± 2.4 ppb (*15*)] reproduce multidecadal-scale variability observed in a shallow core (WDC05A) (*16*) and in the Law Dome ice core (*15*, *17*, *18*). We used the WAIS Divide layer-counted ice chronology (*19*) and a dynamic firn densification model to construct a gas-age chronology. A Monte Carlo correlation technique using the multidecadal variations was then used to create a GISP2 gas-age chronology synchronized with the WAIS Divide chronology (*15*). When the synchronized GISP2 chronology was compared to one constructed independently with a firn densification model and a layer-counted ice chronology, we found a difference of 0 ± 11 years, demonstrating that our chronology is robust (*15*). The IPD was calculated by subtracting the WAIS Divide from the GISP2 CH_4 concentration after linear interpolation to annual spacing. Uncertainty bands (1σ) were computed with a Monte Carlo technique incorporating measurement precision and timescale uncertainties (*15*).

The IPD remains essentially constant (781 B.C.E. to 1803 C.E. mean, 41.6 ppb; trend 0.9 ± 0.3 ppb/ka) throughout the LPIH despite a 115-ppb (17%) increase in the global concentration, which is broadly consistent with previous low-resolution estimates (fig. S4) (*8*, *17*, *20*). The IPD record shows small (~5 ppb) centennial-scale variations, with a minimum around 250 B.C.E. and maximum around 1100 C.E.

We used an Eight Box Atmospheric CH_4 Model (EBAMM) after (*21*) to examine hypothesized CH_4 emission scenarios and to compare modeled concentrations with the ice core records (*15*). The model has six tropospheric boxes covering 30° latitude each and one stratospheric box per hemisphere. We refer to these boxes as the tropical (0° to 30°), mid-latitude (30° to 60°), and high-latitude (60° to 90°) boxes. The distribution of CH_4 sources is fundamentally underconstrained by concentration data from just the two poles (*22*). However, the modern source distribution provides additional constraints on the relatively small emissions from the 30° to 90°S and 60° to 90°N regions (*15*). With these constraints, our data can be used in conjunction with EBAMM to solve for the source strength of two latitudinal bands at a time [fig. S8 (*15*)]. We constructed three "latitudinal" emission scenarios (L1, L2, and L3) that balance the global budget and represent the range of realistic emissions. While keeping emissions outside the zonal bands of interest constant, we solved for emissions in the Southern Hemisphere (SH) versus NH tropics (L1), tropical (30°S to 30°N) versus mid-latitude NH (L2), and tropical versus mid- to high-latitude NH (L3, Fig. 1). Whenever two EBAMM boxes fell within a latitudinal band, we assumed a fixed emission ratio between them. L3 is equivalent to a simpler three-box model (fig. S9) (*8*, *15*). Next, we calculated the net change in emissions between 800 B.C.E. and 1400 C.E. in each latitudinal band, using linear regression (Table 1). We focused on the time period from 800 B.C.E. to 1400 C.E. to avoid the exponential population increase after 1500 C.E. and potential natural emission reductions related to the Little Ice Age. Assuming an atmospheric lifetime of 10 years (*12*), our latitudinal scenarios show that global sources increased by ~24 Tg/year between 800 B.C.E. and 1400 C.E., with the majority of that increase coming from tropical sources (Fig. 1). Varying the CH_4 lifetime from 8 to 12 years (*12*) caused the increase in global emissions to change by ±5 Tg/year but did not affect the latitudinal distribution of CH_4 emissions over the LPIH (*15*).

There are two published model-based scenarios of natural wetland CH_4 emission changes during the LPIH (N1 and N2 in Table 1, and Fig. 2). Scenario N1 is based on TRENCH (Transient Emissions of Natural CH_4), a coarse-grid transient model forced by global ice volume, greenhouse gases, and insolation (*23*). Scenario N2 used output from a fine-grid CH_4 emissions module tied to a dynamic vegetation model, using the climate from the HadCM3 (Hadley Centre Coupled Model, version 3) general circulation model (*3*). These models suggest that global natural CH_4 emissions changed between –2 and 10 Tg/year between 800 B.C.E and 1400 C.E. for the N1 and N2 scenarios, respectively. Neither indicates large

[1]College of Earth, Ocean, and Atmospheric Sciences, Oregon State University, Corvallis, OR 97331, USA. [2]Department of Geosciences and Earth and Environmental Systems Institute, Pennsylvania State University, University Park, PA 16802, USA.

*Corresponding author. E-mail: logan.e.mitchell@gmail.com

decreases in natural CH_4 emissions during the late Holocene in response to declining NH insolation, as proposed by the early anthropogenic hypothesis. However, neither model can explain the global increase in CH_4 emissions of ~24 Tg/year, suggesting that either these models are deficient in some way or some amount of anthropogenic emissions is needed to explain the full LPIH CH_4 increase.

Scenarios A1 and A2 use two published estimates of anthropogenic emissions for the LPIH, while leaving natural emissions constant (to isolate the anthropogenic impact). Scenario A1 uses anthropogenic emission estimates from Houweling *et al.* (*24*) (anthropogenic emissions = 20 Tg/year at 1500 C.E.), and A2 uses estimates from Ruddiman (*25*) (anthropogenic emissions = 43 Tg/year at 1500 C.E.). To estimate time-dependent anthropogenic emissions, we binned global population from the HYDE 3.1 database (*14*) into the EBAMM boxes and defined per-capita emissions based on estimates of emissions and population in 1500 C.E. Scenarios A1 and A2 assume constant per-capita emissions; scenarios involving changes in per-capita emissions from rice agriculture with time are considered below. The latitudinal distribution of CH_4 emissions from rice agriculture was calculated using population from the rice-producing region of Asia (60° to 140°E and 10°S to 50°N) (*4*, *5*). If anthropogenic biomass burning emissions are also scaled on a per-capita basis, the $^{13}CH_4$ isotopic budget increases with time, which is inconsistent with the isotopic observations (*15*, *26*). We therefore kept all biomass burning emissions (natural and anthropogenic) constant; although some small variations are expected based on $\delta^{13}CH_4$ observations (*26*), these lack a long-term trend and cannot be systematically tied to population changes on a per-capita basis (*27*). A1 and A2 yield an increase in emissions of 12 Tg/year and 24 Tg/year from 800 B.C.E. to 1400 C.E., respectively. Because most of the increase in emissions occurred in the NH (Table 1), both scenarios cause the IPD to increase through time, which is not observed in the IPD record (Fig. 2). However, increases in global population followed by losses from the Mongol invasion and the spread of the Black Plague in the rice-producing portion of Asia (fig. S12) create a maximum in the modeled IPD from ~1000 to 1400 C.E., which is observed in the IPD record lending support to the hypothesis that some of the LPIH increases in emissions were anthropogenic in origin and that variability in population is responsible for some of the variations in the CH_4 record (*16*).

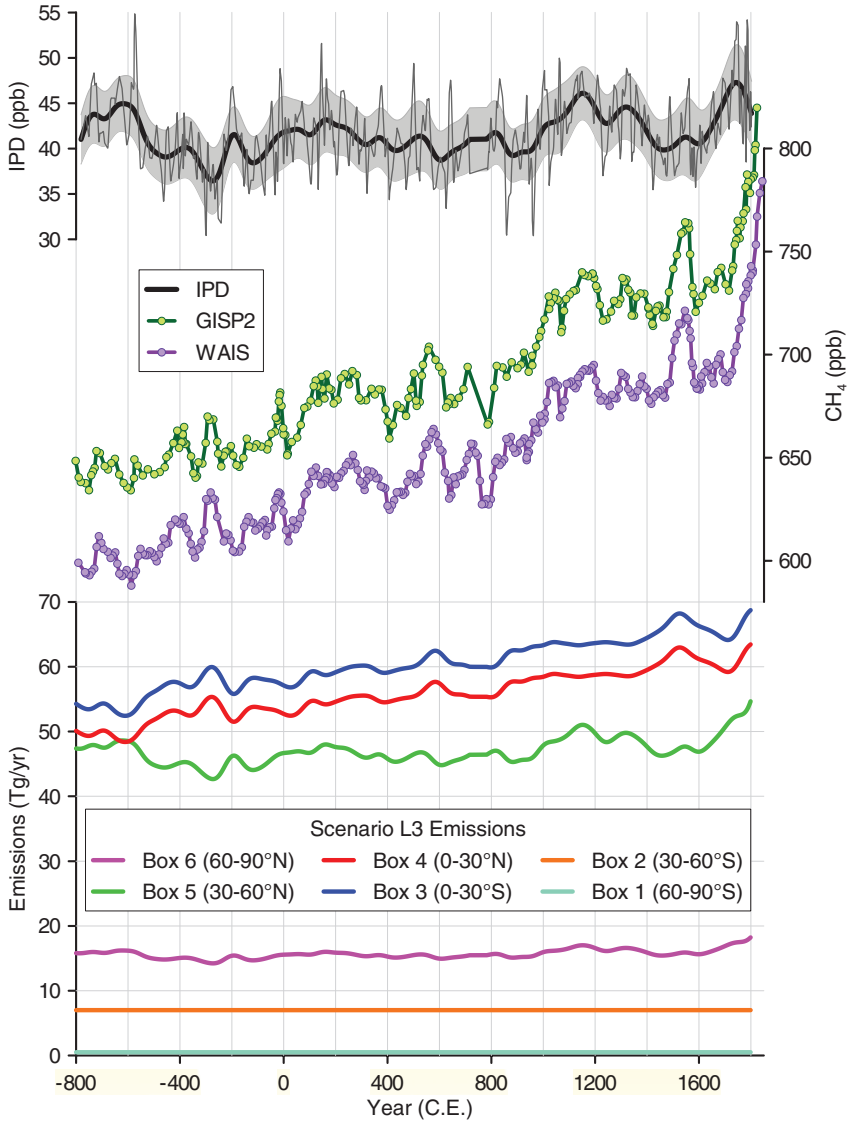

Fig. 1. IPD (top), ice core CH_4 records (middle), and calculated emissions from scenario L3 (bottom). CH_4 data points show the mean concentration from replicate samples measured at that depth. The thin IPD line shows the IPD obtained by linear interpolation between ice core measurements at an annual spacing, and the thick line was computed using a 20-year low-pass filter. The IPD 1σ error bands were obtained using a Monte Carlo procedure accounting for analytical uncertainty of the measurements and chronologic uncertainty of the tie points (*15*).

The contribution of natural versus anthropogenic emissions can be distinguished from their latitudinal distribution (Table 1). Comparing anthropogenic emissions to the emissions in the latitudinal scenarios, it is clear that scenarios A1 and A2 both have moderate NH emissions similar to those of L1, L2, and L3, whereas N1 and N2 do not. This suggests that most of the increase in NH emissions is anthropogenic in origin, particularly in the tropical NH (N2 suggests that a small fraction of the mid-latitude NH increase could be natural). In the SH, A1 and A2 show small increases in emissions, because there are minimal population increases in the SH. However, the primary source increase in scenario N2 is SH tropical wetlands, which is consistent with reconstructed increases in the South American monsoon strength (*28*). Because natural wetlands represent the only sizeable source of SH tropical emissions in any of our scenarios, it follows that they are responsible for the majority of the SH emissions identified by our latitudinal scenarios. Scenario N1 does not show tropical SH increases, possibly because N1 has a lower spatial resolution and simplified climate.

Based on these results, we examined scenarios with combined natural and anthropogenic emissions, as well as the impact of allowing per-capita emissions from rice agriculture to change through time (*29*, *30*). If per-capita emissions from rice agriculture were constant through time, then the best fit to the concentration data is a combination of N2 and A1. However, if we assume that the per-capita emissions from rice agriculture decreased linearly by 50% over the LPIH, then the larger anthropogenic emissions of A2 combined with N2 provide the best fit (Fig. 2). Larger reductions in per-capita emissions from rice agriculture do not fit the concentration data when using our modeling framework (*15*).

Given the current understanding of past population trends and the dependence of CH_4 emissions on climate, our results suggest that increases in both SH natural wetland emissions and a

Table 1. Modeled change in zonal CH_4 emissions between 800 B.C.E. and 1400 C.E. (Tg/year), assuming a 10-year CH_4 lifetime. Model scenario labels are as follows: L1, L2, and L3 solve for total emissions in selected zonal regions indicated by the bold and italic numbers. N1 and N2 have changes in natural emissions only. A1 and A2 have changes in anthropogenic emissions only. The combined scenarios (N2+A1 and N2+A2 with −50% per capita) have changes in both natural and anthropogenic emissions.

EBAMM box (latitude band)	L1*	L2*	L3*	N1	N2	A1	A2	N2+A1	N2+A2 with −50% per capita
6 (60° to 90°N)	0	0	**1** ± **1**	0	−1	0	0	0	0
5 (30° to 60°N)	0	**6** ± **6**	**3** ± **3**	−1	3	4	8	7	6
4 (0° to 30°N)	**18** ± **9**	*9* ± *3*	*9* ± *2*	−1	1	7	15	7	10
3 (0° to 30°S)	*6* ± *7*	*9* ± *3*	*10* ± *2*	0	7	1	1	8	8
2 (30° to 60°S)	0	0	0	0	0	0	0	0	0
1 (60° to 90°S)	0	0	0	0	0	0	0	0	0
Total change	24 ± 4	24 ± 4	23 ± 4	(−2)	10	12	24	22	24
CH_4 increase (ppb)	93	92	92	(−6)	41	43	92	84	94

*The difference in the zonal CH_4 emissions between 800 B.C.E. and 1400 C.E. (±2 times the 1σ SD of the prediction interval) after calculating the linear regression of emissions from the global CH_4 budget solved for tropical and subtropical NH emissions. In L1 to L3, we solved for the zonal bands indicated by the bold and italic numbers; when there were two boxes within a band, we assumed a fixed emission ratio between them. See the supplementary materials for details.

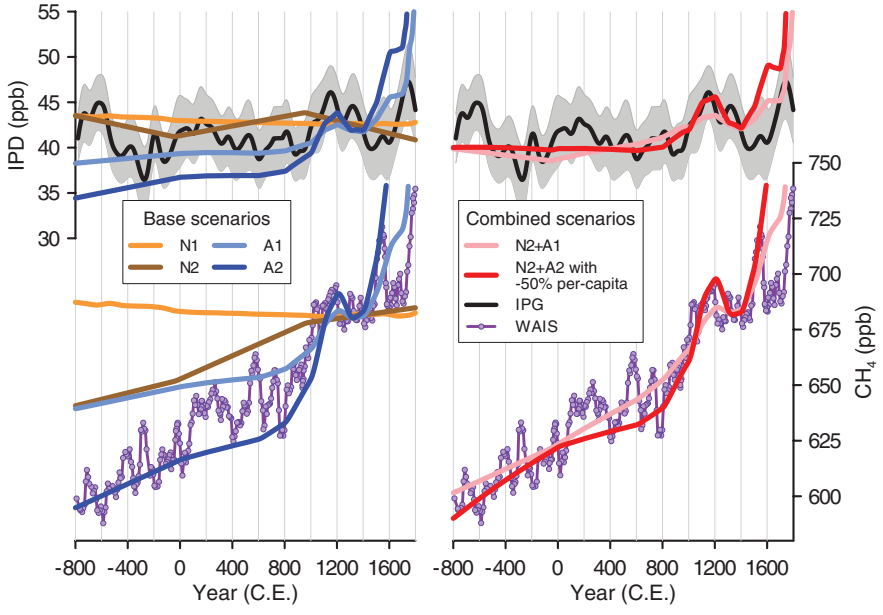

Fig. 2. Modeled CH_4 concentrations from the IPD (top) and box 1 (60° to 90°S, bottom) for scenarios N1, N2, A1, and A2 (left), as well as the combined scenarios A1+N2, and A2+N2 with a 50% reduction in per-capita rice agriculture emissions (right). All scenarios are tuned to match the concentration and IPD at ~1400 C.E. The emission histories used to produce these scenarios are shown in fig. S10. Model concentrations from box 6 (60° to 90°N) and Greenland concentration data are omitted for clarity.

moderate amount of NH anthropogenic emissions are needed to close the LPIH global CH_4 budget. Our concentration data set provides a constraint for future CH_4 budget modeling efforts focusing on constraining natural and anthropogenic emissions.

References and Notes

1. P. Forster *et al.*, in *Climate Change 2007: The Physical Science Basis. Contribution of Working Group I to the Fourth Assessment Report of the Intergovernmental Panel on Climate Change*, S. Solomon *et al.*, Eds. (Cambridge Univ. Press, Cambridge, 2007), pp. 131–234.
2. W. F. Ruddiman, *Clim. Change* **61**, 261–293 (2003).
3. J. S. Singarayer, P. J. Valdes, P. Friedlingstein, S. Nelson, D. J. Beerling, *Nature* **470**, 82–85 (2011).
4. D. Q. Fuller *et al.*, *Holocene* **21**, 743–759 (2011).
5. W. F. Ruddiman, Z. T. Guo, X. Zhou, H. B. Wu, Y. Y. Yu, *Quat. Sci. Rev.* **27**, 1291–1295 (2008).
6. W. F. Ruddiman, J. E. Kutzbach, S. J. Vavrus, *Holocene* **21**, 865–8879 (2011).
7. I. Fung *et al.*, *J. Geophys. Res. Atmos.* **96**, 13033 (1991).
8. J. Chappellaz *et al.*, *J. Geophys. Res. Atmos.* **102**, 15987 (1997).
9. E. J. Brook, S. Harder, J. Severinghaus, E. J. Steig, C. M. Sucher, *Global Biogeochem. Cycles* **14**, 559–572 (2000).
10. K. R. Lassey, D. M. Etheridge, D. C. Lowe, A. M. Smith, D. F. Ferretti, *Atmos. Chem. Phys.* **7**, 2119–2139 (2007).
11. S. A. Montzka *et al.*, *Science* **331**, 67–69 (2011).
12. V. Naik *et al.*, *Atmos. Chem. Phys.* **13**, 5277–5298 (2013).
13. E. J. Dlugokencky *et al.*, *Geophys. Res. Lett.* **36**, L18803 (2009).
14. K. K. Goldewijk, A. Beusen, P. Janssen, *Holocene* **20**, 565–573 (2010).
15. Materials and methods are available as supplementary materials on *Science* Online.
16. L. E. Mitchell, E. J. Brook, T. Sowers, J. R. McConnell, K. Taylor, *J. Geophys. Res. Biogeosci.* **116**, G02007 (2011).
17. D. M. Etheridge, L. P. Steele, R. J. Francey, R. L. Langenfelds, *J. Geophys. Res. Atmos.* **103**, 15979 (1998).
18. C. MacFarling Meure *et al.*, *Geophys. Res. Lett.* **33**, L14810 (2006).
19. T. J. Fudge *et al.*, *Nature* **500**, 440–444 (2013).
20. T. Nakazawa *et al.*, *Geophys. Res. Lett.* **20**, 943–946 (1993).
21. T. Marik, thesis, University of Heidelberg, Heidelberg, Germany (1998).
22. M. A. K. Khalil, R. A. Rasmussen, *J. Geophys. Res. Oceans* **88**, 5131 (1983).
23. T. Y. M. Konijnendijk, S. L. Weber, E. Tuenter, M. van Weele, *Clim. Past.* **7**, 635–648 (2011).
24. S. Houweling, F. Dentener, J. Lelieveld, *J. Geophys. Res. Atmos.* **105**, 17243 (2000).
25. W. F. Ruddiman, *Rev. Geophys.* **45**, RG4001 (2007).
26. C. J. Sapart *et al.*, *Nature* **490**, 85–88 (2012).
27. O. Pechony, D. T. Shindell, *Proc. Natl. Acad. Sci. U.S.A.* **107**, 19167–19170 (2010).
28. X. F. Wang *et al.*, *Quat. Sci. Rev.* **25**, 3391–3403 (2006).
29. W. F. Ruddiman, E. C. Ellis, *Quat. Sci. Rev.* **28**, 3011–3015 (2009).
30. J. O. Kaplan *et al.*, *Holocene* **21**, 775–791 (2011).
31. L. E. Mitchell, thesis, Oregon State University, Corvallis, OR (2013).

Acknowledgments: This work was supported by NSF Office of Polar Programs (OPP) grants 0538578, 0520523, 0944584, and 0538538; and by NASA/Oregon Space Grant Consortium grant NNG05GJ85H and the NOAA Climate and Global Change Fellowship Program, administered by the University Corporation for Atmospheric Research (C.B.). We thank two anonymous reviewers whose comments greatly improved the manuscript; B. Markle, A. Morin, B. Williams, and J. Edwards for assisting in sample preparation and analysis; T. Marik, who provided the original eight-box model code (BOSCAGE); J. Severinghaus and G. Etiope, who contributed preliminary results from their work; T. Konijnendijk, J. Van Etten, and J. Singarayer, who provided model data from their published works; the WAIS Divide Science Coordination Office at the Desert Research Institute, Reno, NV for the collection and distribution of the WAIS Divide ice core (K. Taylor, NSF grants 0230396, 0440817, 0944348, and 0944266–University of New Hampshire); NSF OPP, which funds the Ice Drilling Program Office and Ice Drilling Design and Operations group for coring activities; NSF, which funds the National Ice Core Laboratory, which curated and processed the core; Raytheon Polar Services, which provided logistics support in Antarctica; and the 109th New York Air National Guard for airlift in Antarctica. Data and description can be downloaded from the NOAA National Climate Data Center (www.ncdc.noaa.gov/paleo/paleo.html). EBAMM model code is archived with L.E.M.'s thesis (*31*), available online at http://ir.library.oregonstate.edu/xmlui/handle/1957/37906.

Supplementary Materials

www.sciencemag.org/content/342/6161/964/suppl/DC1
Materials and Methods
Figs. S1 to S17
Tables S1 and S2
References

9 April 2013; accepted 23 October 2013
10.1126/science.1238920